

The interactions between shear bands and rigid lamellar inclusions in a ductile metal matrix

BY FRANCESCO DAL CORSO AND DAVIDE BIGONI*

*Department of Mechanical and Structural Engineering, University of Trento,
via Mesiano 77, 38050 Trento, Italy*

A ductile metal matrix (modelled as a nonlinear elastic material) containing a dilute suspension of an iso-oriented lamellar stiff phase (modelled as stiffeners, i.e. zero thickness, rigid inclusions) is subject to a simple shear of finite amount, parallel to the inclusion orientation, and subsequently perturbed through an incremental Mode I loading, uniform at infinity. Solution to this problem permits analytical investigations of the emergence of shear bands and their interaction with a rigid inclusion (involving a stress square-root singularity at its tip) and discloses the mechanisms of ductile failure in reinforced materials (explaining for instance the experimental evidence that shear bands tend to nucleate and grow parallel to thin hard inclusions). Finally, investigated beyond the elliptic range, the obtained solution becomes non-unique and reveals non-decay and singularity of the fields, facts that provide analytical justification for the difficulties associated with numerical treatment of shear bands.

Keywords: stiffener; anticrack; localized deformations; residual stress

1. Introduction

Experimental evidence in ductile matrix materials containing a second stiff phase shows that localized deformations in the form of shear bands nucleate at inclusion boundaries, where they grow and subsequently develop complex interactions between themselves and the second phase. Therefore, the presence of defects is crucially important in the understanding of failure in ductile matrix composites, particularly when defects involve stress concentrations, as is the case of the lamellar suspensions experimentally investigated in metals ([Öztürk *et al.* 1991](#)), plastics ([Bigoni *et al.* 2008](#)) and rocks ([Misra & Mandal 2007](#)). In these composites, only an analytical solution can detail the structure of singularities related to the sharpness of both lamellae and shear bands, while numerical approaches can hardly have the necessary resolution. The objective of the present article is to derive one such solution, through a generalization of results obtained by [Dal Corso *et al.* \(2008\)](#), and to employ it to investigate the complex interaction between singularities and shear bands at the inclusion tip. To this purpose, a rigid line inclusion, a so-called ‘stiffener’, is analysed embedded in an elastic incompressible infinite material (in the examples we will refer to a

* Author for correspondence (bigoni@ing.unitn.it).

J_2 -deformation theory material) deformed under plane strain. The medium is assumed to be subject to a simple shear deformation of finite amount parallel to the inclusion line, which generates a uniform state of strain and stress, both having principal directions *inclined* with respect to the stiffener line. Taking this configuration as reference in a relative Lagrangian description, the response is analysed to an incremental uniform Mode I loading at infinity,¹ so that the solution can be explored near the border of ellipticity loss, where the incremental fields are shown to self-organize along shear bands.

The obtained Mode I loading analytical solution shows the development of two shear bands, with, for low hardening, the one closest in alignment with the stiffener being the more pronounced.² Therefore, a stiffener embedded in a low hardening matrix tends to focus the deformation parallel to its line, a finding substantiated by the experimental results of Misra & Mandal (2007), referring to geological formations and to models prepared with polymethylmethacrylate containing metal inclusions.³

Finally, accepting the fact that decay of the incremental fields does not occur and incremental strain and stress becomes infinite along certain shear band directions, the obtained solution is extended and investigated outside ellipticity, namely, in the parabolic and hyperbolic regimes. Here, it is shown that the solution is not unique, so that one, two, three or four (one or two) differently inclined shear bands are predicted to become possible in the hyperbolic (parabolic) range. This result substantiates with an analytical solution the well-known difficulties connected to the numerical treatment of ill-posed (i.e. non-elliptic) boundary-value problems.

2. Stiffener neutrality during simple shear of an elastic material

With reference to figure 1, a block of a material is subject to a simple shear deformation when two displacement components are null (along axes \hat{x}_2 and \hat{x}_3) and the other component, \hat{u}_1 , depends linearly only on \hat{x}_2^0 , namely

$$\hat{u}_1(\hat{x}_2^0) = \gamma \hat{x}_2^0 \quad \text{and} \quad \hat{u}_2 = \hat{u}_3 = 0, \quad (2.1)$$

so that, if a point at $\hat{x}_2^0 = h$ horizontally displaces of s , we can determine the dimensionless parameter $\gamma = s/h$, controlling the amplitude of shear deformation.

¹ Since the state of prestress is arbitrarily inclined with respect to the inclusion line, the solution obtained in the present article generalizes that previously given by Dal Corso *et al.* (2008), where a stiffener aligned parallel to the principal axes of prestress has been considered. Note that Mode I loading is defined with respect to the axes parallel and orthogonal to the stiffener.

² Differently from results presented by Bigoni *et al.* (2008), now the two axial symmetries are lost, so that the shear bands are not symmetrical with respect to the stiffener line and one of the two becomes a preferential failure mode.

³ We include in appendix B of this article, the solution where a stiffener is forced to incrementally rotate (through application of an external incremental bending moment) by a given amount, a problem modelling the mechanical fields generated through the so-called ‘vane test’ in soil mechanics. Differently from the case when the inclusion is embedded in a matrix and loaded at infinity, in this situation, we show that the two shear bands more inclined with respect to the stiffener become the preferred failure modes.

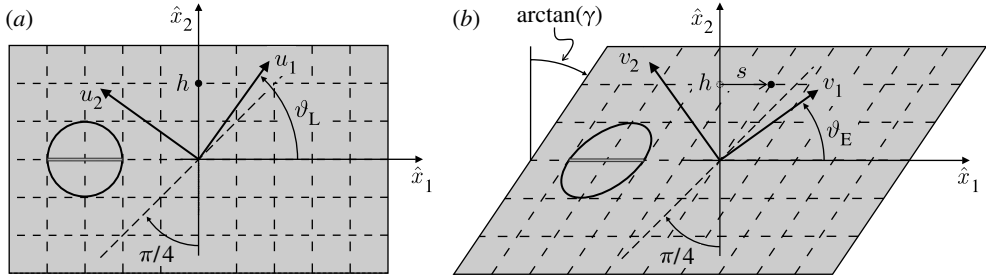


Figure 1. Simple shear deformation ($\arctan \gamma = 34^\circ$ has been assumed in the sketch, so that $\vartheta_L \approx 54.318^\circ$ and $\vartheta_E \approx 35.682^\circ$). (a) Reference configuration and (b) configuration at a shear amount $\gamma = s/h$, with indicated Lagrangian and Eulerian principal axes, inclined at ϑ_L and ϑ_E , respectively. Note that the circle in the reference configuration becomes a strain ellipse in the deformed configuration, so that a stiffener parallel to the \hat{x}_1 -axis leaves the material unperturbed at every stage of the simple shear deformation.

The left (B) and right (C) Cauchy–Green deformation tensors can be calculated from the displacement field (2.1) and result in

$$\left. \begin{aligned} \mathbf{B} &= \mathbf{I} + \gamma(\hat{e}_1 \otimes \hat{e}_2 + \hat{e}_2 \otimes \hat{e}_1) + \gamma^2 \hat{e}_1 \otimes \hat{e}_1 \\ \mathbf{C} &= \mathbf{I} + \gamma(\hat{e}_1 \otimes \hat{e}_2 + \hat{e}_2 \otimes \hat{e}_1) + \gamma^2 \hat{e}_2 \otimes \hat{e}_2, \end{aligned} \right\} \quad (2.2)$$

and

where \hat{e}_1 and \hat{e}_2 are the two unit vectors parallel to the \hat{x}_1 and \hat{x}_2 axes, respectively.

The eigenvectors of **B** and **C** define the principal Eulerian and Lagrangian axes, so that in the \hat{x}_1 – \hat{x}_2 plane these are

$$\left. \begin{aligned} \{\mathbf{v}_j\} &= \frac{1}{\sqrt{4 + [\gamma - (-1)^j \sqrt{4 + \gamma^2}]^2}} \left\{ \gamma - (-1)^j \sqrt{4 + \gamma^2}, 2 \right\} \\ \{\mathbf{u}_j\} &= \frac{1}{\sqrt{4 + [\gamma + (-1)^j \sqrt{4 + \gamma^2}]^2}} \left\{ -\gamma - (-1)^j \sqrt{4 + \gamma^2}, 2 \right\}, \end{aligned} \right\} \quad (2.3)$$

and

(where $j=1, 2$) respectively, while the principal stretches result is given by

$$\lambda_j = -(-1)^j \frac{\gamma}{2} + \sqrt{1 + \left(\frac{\gamma}{2}\right)^2}, \quad (2.4)$$

where $j=1, 2$. Note that

$$\lambda_1 - \lambda_2 = \gamma, \quad (2.5)$$

so that if $\gamma > 0$ (< 0) then $\lambda_1 > \lambda_2$ ($\lambda_1 < \lambda_2$).

The eigenvectors (2.3) yield the inclination of the Eulerian, ϑ_E , and Lagrangian, ϑ_L , axes with respect to the \hat{x}_1 -axis

$$\vartheta_E = \frac{1}{2} \arctan\left(\frac{2}{\gamma}\right) \quad \text{and} \quad \vartheta_L = \frac{\pi}{2} - \vartheta_E. \quad (2.6)$$

With reference to the Cauchy–Green deformation tensors (2.2), we note that a fibre parallel to the \hat{x}_1 -axis, singled out by the unit vector \hat{e}_1 remains unstretched, since

$$\hat{e}_1 \cdot \mathbf{C} \hat{e}_1 = \hat{e}_1 \cdot \mathbf{B}^{-1} \hat{e}_1 = 1, \tag{2.7}$$

so that the fibres parallel to the \hat{x}_1 -axis in figure 1 are so-called ‘zero elongation lines’ (Weissenberg 1948). As a conclusion, a stiffener parallel to the shear deformation leaves the material unperturbed.

For a material isotropic in the reference configuration, the Cauchy stress is coaxial to the left Cauchy–Green deformation tensor \mathbf{B} , so that in the Eulerian principal reference system we have the spectral representation

$$\mathbf{T} = T_1 \mathbf{v}_1 \otimes \mathbf{v}_1 + T_2 \mathbf{v}_2 \otimes \mathbf{v}_2 + T_3 \mathbf{e}_3 \otimes \mathbf{e}_3, \tag{2.8}$$

where, in the \hat{x}_1 – \hat{x}_2 reference system, the unit vectors \mathbf{v}_1 and \mathbf{v}_2 , equations (2.3)₁, are now defined by the components

$$\{\mathbf{v}_1\} = \{\cos \vartheta_E, \sin \vartheta_E\} \quad \text{and} \quad \{\mathbf{v}_2\} = \{-\sin \vartheta_E, \cos \vartheta_E\}. \tag{2.9}$$

Therefore, in the \hat{x}_1 – \hat{x}_2 reference system, we have

$$\left. \begin{aligned} \hat{T}_{11} &= T_1 \cos^2 \vartheta_E + T_2 \sin^2 \vartheta_E, & \hat{T}_{22} &= T_1 \sin^2 \vartheta_E + T_2 \cos^2 \vartheta_E \\ \text{and} & & & \\ \hat{T}_{12} &= \frac{T_1 - T_2}{2} \sin 2\vartheta_E, & & \end{aligned} \right\} \tag{2.10}$$

from which the well-known ‘universal relation’

$$\hat{T}_{11} - \hat{T}_{22} = \gamma \hat{T}_{12} \tag{2.11}$$

is obtained.

Although all the subsequent developments are fully general, we will refer in the examples to a J_2 -deformation theory material defined by the power-law strain energy density

$$W = \frac{K}{N+1} \epsilon_e^{N+1}, \tag{2.12}$$

where K is a positive stiffness parameter; $N \in]0,1]$ is the strain-hardening exponent; and ϵ_e is the effective strain that, for the plane strain case, reduces to

$$\epsilon_e = \frac{2}{\sqrt{3}} |\epsilon|, \tag{2.13}$$

in which $\epsilon = \epsilon_1 = \log \lambda_1$ is the logarithmic stretch, a function of γ through equation (2.4). For a J_2 -deformation theory material, we obtain

$$\left. \begin{aligned} \hat{T}_{11} \\ \hat{T}_{22} \end{aligned} \right\} = p \pm \frac{\mu \gamma}{\sqrt{4 + \gamma^2} \coth 2\epsilon}, \quad \hat{T}_{12} = \frac{4\mu_* \epsilon}{N \sqrt{4 + \gamma^2}} \quad \text{and} \quad T_3 = p, \tag{2.14}$$

where p is the mean stress and μ and μ_* are incremental shear moduli that depend on the current stretch in the following way:⁴

$$\mu = \mu_0 2\epsilon |\epsilon|^{N-1} \coth 2\epsilon \quad \text{and} \quad \mu_* = N \mu_0 |\epsilon|^{N-1}, \tag{2.15}$$

⁴Note that the J_2 -deformation theory material is a nonlinear elastic material isotropic in the unloaded state. Owing to the fact that the incremental shear moduli μ and μ_* tend to infinity when ϵ tends to zero (and $N < 1$), the ratio μ_*/μ tends to N (and therefore is different from 1).

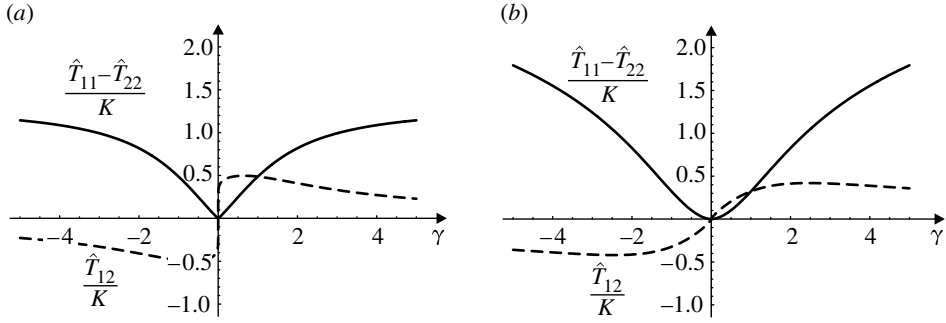


Figure 2. Simple shear of an elastic, incompressible, J_2 -deformation theory material: stress response for finite-shear-amplitude γ at (a) low ($N=0.1$) and (b) high ($N=0.8$) strain hardening.

where

$$\mu_0 = \frac{K}{3} \left(\frac{2}{\sqrt{3}} \right)^{N-1}. \quad (2.16)$$

Considering small shear amplitude γ , the constitutive relations (2.14) become

$$\left. \begin{matrix} \hat{T}_{11} \\ \hat{T}_{22} \end{matrix} \right\} = p \pm \frac{\mu_0}{2^N} |\gamma|^{N+1} \quad \text{and} \quad \hat{T}_{12} = \text{sign}(\gamma) \frac{\mu_0}{2^{N-1}} |\gamma|^N. \quad (2.17)$$

The deviatoric stress and the shear stress, made dimensionless through division by K , are reported in figure 2 for a J_2 -deformation theory material, at (a) low ($N=0.1$) and (b) high ($N=0.8$) strain hardening. Note that it is evident from equation (2.17), that for $\gamma=0$, the curve representing the deviatoric stress has a horizontal tangent and the curve representing the shear stress has a vertical tangent. Although the vertical tangent is not visible in figure 2b, it is easy to check its existence; in fact, the incremental equations corresponding to equation (2.17) become

$$\dot{T}_{11} = \dot{T}_{22} = \dot{p} \quad \text{and} \quad \dot{T}_{12} = \mu_* \dot{\gamma}, \quad (2.18)$$

where $\dot{\gamma}$ (\dot{p}) represents the shear (mean stress) increment and μ_* tends to infinity when γ tends to zero. Moreover, the curve relative to $N=0.1$ coincides with that plotted by Harren *et al.* (1989, fig. 2).

3. Mode I perturbation of an elastic infinite medium prestressed through a finite shear parallel to an embedded stiffener

A rigid-line inclusion is analysed embedded in an elastic material, homogeneously prestressed within the elliptic regime by a simple shear and subject to an incremental Mode I deformation uniform at infinity (for uniform Mode II loading, the stiffener leaves the medium unperturbed). We start by briefly introducing the incremental constitutive equations.

(a) Incremental constitutive equations

The incremental response of an incompressible, nonlinear elastic material homogeneously deformed under a plane strain condition, can be described through the linear relation (Bigoni & Dal Corso 2008)

$$\dot{\mathbf{t}} = \mathbb{K}[\nabla \mathbf{v}^T] + \dot{p} \mathbf{I}, \quad (3.1)$$

where $(\cdot)^T$ denotes the transpose; $\dot{\mathbf{t}}$ is the increment of the nominal (unsymmetrical) stress tensor \mathbf{t} ; $\nabla \mathbf{v}$ is the gradient of incremental displacement (satisfying the incompressibility constraint $\text{tr } \nabla \mathbf{v} = 0$); and \dot{p} is the incremental in-plane mean stress. The fourth-order constitutive tensor \mathbb{K} , describing orthotropy (aligned parallel to the current principal stress directions), is a function of the current state of stress, and its components \mathbb{K}_{ijkl} (for instance given by [Bigoni & Dal Corso 2008](#)) are functions of the following dimensionless quantities:

$$\xi = \frac{\mu_*}{\mu}, \quad \eta = \frac{T_1 + T_2}{2\mu} \quad \text{and} \quad k = \frac{T_1 - T_2}{2\mu}, \quad (3.2)$$

where T_1 and T_2 are the principal components of Cauchy stress and μ and μ_* describe the material response to shear (μ for shear parallel and μ_* for shear inclined at $\pi/4$ with respect to T_1), and may be arbitrary functions of the current stress and/or strain.

For a J_2 -deformation theory material, the dimensionless constants $(3.2)_{1,3}$ are related to the principal stretch in the x_1 -direction, namely λ_1 , through the relations

$$\xi = \frac{N(\lambda_1^4 - 1)}{2(\log \lambda_1)(\lambda_1^4 + 1)} \quad \text{and} \quad k = \frac{\lambda_1^4 - 1}{\lambda_1^4 + 1}, \quad (3.3)$$

while the in-plane stress parameter η remains unprescribed.

Introducing a stream function $\psi(z) = \psi(x_1 + \Omega x_2)$ with the property

$$v_1 = \frac{\partial \psi}{\partial x_2} \quad \text{and} \quad v_2 = -\frac{\partial \psi}{\partial x_1} \quad (3.4)$$

(so that the incompressibility condition is automatically satisfied), the differential equations governing incremental equilibrium yield the values of the roots Ω_j satisfying

$$\Omega_j^2 = \frac{1 - 2\xi + (-1)^j \sqrt{4\xi^2 - 4\xi + k^2}}{1 - k} \quad (j = 1, \dots, 4). \quad (3.5)$$

According to the nature assumed by roots Ω_j as a function of parameters ξ and k , the incremental problem can be classified as elliptic (E), parabolic (P) and hyperbolic (H) (see for instance [Bigoni & Dal Corso 2008](#), fig. 2). In particular, defining

$$\Omega_j = \alpha_j + i\beta_j, \quad (3.6)$$

where $i = \sqrt{-1}$ is the imaginary unit and $\alpha_j = \text{Re}[\Omega_j]$ and $\beta_j = \text{Im}[\Omega_j]$ ($\text{Re}[\cdot]$ and $\text{Im}[\cdot]$ denote the real and imaginary part of the relevant argument), the elliptic regime corresponds to

$$\beta_j \neq 0 \quad (j = 1, \dots, 4). \quad (3.7)$$

We define the elliptic imaginary (EI) regime as

$$k^2 < 1 \quad \text{and} \quad 2\xi > 1 + \sqrt{1 - k^2}, \quad (3.8)$$

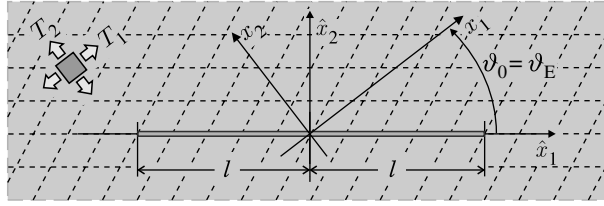


Figure 3. The rigid-line inclusion (of length $2l$) in an infinite material deformed under simple shear parallel to the inclusion. The state of stress generated at a certain deformation γ has principal values inclined with respect to the \hat{x}_1 - \hat{x}_2 reference system at an angle ϑ_0 taken equal to ϑ_E (although this identification is not necessary in the calculations).

where there are four imaginary conjugate roots Ω_j , so that

$$\alpha_1 = \alpha_2 = 0 \quad \text{and} \quad \left. \begin{matrix} \beta_1 \\ \beta_2 \end{matrix} \right\} = \sqrt{\frac{2\xi - 1 \pm \sqrt{4\xi^2 - 4\xi + k^2}}{1 - k}} > 0, \quad (3.9)$$

and the elliptic complex (EC) regime as

$$k^2 < 1 \quad \text{and} \quad 1 - \sqrt{1 - k^2} < 2\xi < 1 + \sqrt{1 - k^2}, \quad (3.10)$$

where there are four complex conjugate roots Ω_j , so that

$$\left. \begin{matrix} \beta = \beta_1 = \beta_2 \\ \alpha = -\alpha_1 = \alpha_2 \end{matrix} \right\} = \sqrt{\frac{\sqrt{1 - k^2} \pm (2\xi - 1)}{2(1 - k)}} > 0. \quad (3.11)$$

Considering now a \hat{x}_1 - \hat{x}_2 reference system rotated at an angle ϑ_0 with respect to the x_1 - x_2 axes defining the prestress directions and the orthotropy axes (figure 3), the linear constitutive relation (3.1) becomes

$$\hat{\mathbf{t}} = \hat{\mathbb{K}}[\hat{\nabla}\hat{\mathbf{v}}^T] + \hat{p}\mathbf{I}, \quad (3.12)$$

where the nominal stress increment, incremental displacement and its gradient, and the constitutive tensor can be expressed in the \hat{x}_1 - \hat{x}_2 reference system as

$$\hat{\mathbf{t}} = \mathbf{Q}^T \mathbf{t} \mathbf{Q}, \quad \hat{\nabla}\hat{\mathbf{v}} = \mathbf{Q}^T \nabla \mathbf{v} \mathbf{Q} \quad \text{and} \quad \hat{\mathbb{K}}_{ijkl} = Q_{li} Q_{mj} \mathbb{K}_{lmno} Q_{nh} Q_{ok}, \quad (3.13)$$

through the rotation \mathbf{Q} defined as

$$[\mathbf{Q}] = \begin{bmatrix} \cos \vartheta_0 & \sin \vartheta_0 \\ -\sin \vartheta_0 & \cos \vartheta_0 \end{bmatrix}. \quad (3.14)$$

In the \hat{x}_1 - \hat{x}_2 reference system, the stream function employed in equation (3.4) becomes $\hat{\psi}(\hat{z})$, where

$$\hat{z}_j = \hat{x}_1 + W_j \hat{x}_2, \quad W_j = \frac{\sin \vartheta_0 + \Omega_j \cos \vartheta_0}{\cos \vartheta_0 - \Omega_j \sin \vartheta_0} \quad (j = 1, \dots, 4), \quad (3.15)$$

and the property (3.4) now becomes

$$\hat{v}_1 = \frac{\partial \hat{\psi}}{\partial \hat{x}_2} \quad \text{and} \quad \hat{v}_2 = -\frac{\partial \hat{\psi}}{\partial \hat{x}_1}, \quad (3.16)$$

from which the incremental strain and stress fields can be obtained directly in the \hat{x}_1 - \hat{x}_2 reference system.

(b) *Incremental perturbed solution*

A rigid line inclusion of length $2l$ is considered embedded in an elastic material, which is subject to a uniform state of prestress produced by a simple shear parallel to the inclusion and defined by the shear amount γ . The homogeneous state of prestress has the principal stress axes inclined by ϑ_E , equation (2.6), with respect to the inclusion line and is taken as the reference state⁵ on which a perturbation corresponding to remote uniform Mode I incremental deformation $\hat{v}_{2,2}^\infty$ is superimposed.

A \hat{x}_1 - \hat{x}_2 reference system located at the stiffener centre, taken with the inclusion line parallel to the \hat{x}_1 -axis, is inclined at an angle ϑ_0 (taken equal to ϑ_E) with respect to the x_1 - x_2 system, defining the principal stress directions, as shown in figure 3.

The kinematical boundary conditions for a stiffener express the fact that this can only suffer an incremental rigid-body motion

$$\left. \begin{aligned} \hat{v}_1(\hat{x}_1, 0) &= \hat{v}_1(0, 0), \\ \hat{v}_2(\hat{x}_1, 0) &= \hat{v}_2(0, 0) + \omega_S \hat{x}_1, \end{aligned} \right\} \quad \forall |\hat{x}_1| < l, \quad (3.17)$$

so that $\hat{v}_1(0, 0)$, $\hat{v}_2(0, 0)$ and ω_S represent unknown quantities to be determined as a part of the solution, by imposing boundary conditions to ensure equilibrium of the stiffener in terms of incremental ‘global’ axial and shear forces, and incremental moment, respectively,

$$\left. \begin{aligned} \dot{\mathcal{N}} &= \int_{-l}^l \llbracket \hat{t}_{21}(y, 0) \rrbracket dy = 0, \\ \dot{\mathcal{T}} &= \int_{-l}^l \llbracket \hat{t}_{22}(y, 0) \rrbracket dy = 0, \\ \dot{\mathcal{M}} &= \int_{-l}^l \llbracket \hat{t}_{22}(y, 0) \rrbracket y dy = 0, \end{aligned} \right\} \quad (3.18)$$

where the brackets $\llbracket \cdot \rrbracket$ denote the jump in the relevant argument, taken across the stiffener.

Owing to central symmetry considerations (with respect to the stiffener centre) involved in the far-field loading problem under analysis and the specific form of solution sought in the following, the boundary conditions (3.17) and (3.18) can be reduced to the following homogeneous incremental displacement gradient conditions:

$$\left. \begin{aligned} \hat{v}_{1,1}(\hat{x}_1, 0) &= 0, \\ \hat{v}_{2,1}(\hat{x}_1, 0) &= \omega_S, \end{aligned} \right\} \quad \forall |\hat{x}_1| < l, \quad (3.19)$$

⁵The analysis will be carried out with respect to a generic, uniform state of prestress (with principal values inclined at ϑ_0 different from ϑ_E), not necessarily generated through a simple shear deformation.

plus the requirement that the normal stress increment \hat{t}_{22} be continuous across the stiffener

$$\llbracket \hat{t}_{22}(\hat{x}_1, 0) \rrbracket = 0, \quad \forall |\hat{x}_1| < l, \quad (3.20)$$

a condition allowing determination of ω_S .

Prescribing an incremental deformation $\hat{v}_{2,2}^\infty$ at infinity and proceeding in analogy to the crack and shear band problems analysed by Bigoni & Dal Corso (2008), the stream function of the perturbed problem $\hat{\psi}^\circ$ can be sought in the form⁶

$$\hat{\psi}^\circ(\hat{x}_1, \hat{x}_2) = \frac{\hat{v}_{2,2}^\infty}{2} \sum_{j=1}^2 \operatorname{Re} \left\{ D_j \left[\hat{z}_j^2 - \hat{z}_j \sqrt{\hat{z}_j^2 - l^2} + l^2 \ln \left(\hat{z}_j + \sqrt{\hat{z}_j^2 - l^2} \right) \right] \right\}, \quad (3.21)$$

satisfying automatically the decaying condition on the velocity, incremental strain and stress at infinity (in the elliptic regime) and providing a stress square-root singularity at the stiffener tips.

Imposing the stream function (3.21) to satisfy the boundary conditions along the stiffener line (3.19) and (3.20) yields the following linear problem for the complex constants D_1 and D_2 :

$$\begin{bmatrix} \operatorname{Re}[W_1] & -\operatorname{Im}[W_1] & \operatorname{Re}[W_2] & -\operatorname{Im}[W_2] \\ \operatorname{Im}[W_1] & \operatorname{Re}[W_1] & \operatorname{Im}[W_2] & \operatorname{Re}[W_2] \\ 0 & 1 & 0 & 1 \\ -c_{21} & c_{11} & -c_{22} & c_{12} \end{bmatrix} \begin{bmatrix} \operatorname{Re}[D_1] \\ \operatorname{Im}[D_1] \\ \operatorname{Re}[D_2] \\ \operatorname{Im}[D_2] \end{bmatrix} = \begin{bmatrix} 1 \\ 0 \\ 0 \\ 0 \end{bmatrix}, \quad (3.22)$$

where the real constants c_{1j} and c_{2j} ($j=1, \dots, 4$) are defined as

$$\left. \begin{aligned} 2\mu c_{1j} = & \hat{\mathbb{K}}_{1112} - \hat{\mathbb{K}}_{1222} - \operatorname{Re}[W_j] \left[\hat{\mathbb{K}}_{1111} - 2\hat{\mathbb{K}}_{1122} - \hat{\mathbb{K}}_{1221} + \hat{\mathbb{K}}_{2222} \right. \\ & + \operatorname{Re}[W_j] \left(2\hat{\mathbb{K}}_{1121} - 2\hat{\mathbb{K}}_{2122} + \operatorname{Re}[W_j] \hat{\mathbb{K}}_{2121} \right) \\ & \left. + \operatorname{Im}[W_j]^2 \left(2\hat{\mathbb{K}}_{1121} - 2\hat{\mathbb{K}}_{2122} + 3 \operatorname{Re}[W_j] \hat{\mathbb{K}}_{2121} \right) \right] \end{aligned} \right\} \quad (3.23)$$

and

$$\left. \begin{aligned} 2\mu c_{2j} = & \operatorname{Im}[W_j] \left[\hat{\mathbb{K}}_{1111} - 2\hat{\mathbb{K}}_{1122} - \hat{\mathbb{K}}_{1221} + \hat{\mathbb{K}}_{2222} \right. \\ & \left. + \operatorname{Re}[W_j] \left(4\hat{\mathbb{K}}_{1121} - 4\hat{\mathbb{K}}_{2122} + 3 \operatorname{Re}[W_j] \hat{\mathbb{K}}_{2121} \right) - \operatorname{Im}[W_j]^2 \hat{\mathbb{K}}_{2121} \right], \end{aligned} \right\}$$

and depend on the stiffener inclination ϑ_0 and on the prestress and orthotropy parameters ξ , k and η .

We introduce the normalized stiffener rotation Γ as

$$\Gamma = \frac{\omega_S}{\hat{v}_{2,2}^\infty} = -\operatorname{Re}[D_1 + D_2], \quad (3.24)$$

⁶The stream function (3.21) enforces continuity in displacement (or in tractions for fracture mechanics problems) along the branch cut ($|\hat{x}_1| < l$, $\hat{x}_2 = 0$), when appropriate values of the complex constants D_j are chosen. This property remains valid independently of the regime considered.

and since analytical proof looks awkward, we have numerically checked that (i) the solution of the present problem is independent of the in-plane stress parameter η , (ii) the coefficients D_j ($j=1, 2$) solving system (3.22) satisfy the following two equations:

$$\left. \begin{aligned} W_1^2 D_1 + W_2^2 D_2 &= W_1 + W_2 + \Gamma W_1 W_2 \\ W_1^3 D_1 + W_2^3 D_2 &= W_1^2 + W_1 W_2 + W_2^2 + \Gamma W_1 W_2 (W_1 + W_2), \end{aligned} \right\} \quad (3.25)$$

and (iii) the normalized stiffener rotation Γ (3.24) satisfies the conditions

$$\left. \begin{aligned} \Gamma(k=0, \vartheta_0) &= \Gamma(k, \vartheta_0=0) = \Gamma(k, \vartheta_0=\pi/2) = 0 \\ \Gamma &= \Gamma(k, \vartheta_0) = -\Gamma(-k, \pi/2 - \vartheta_0). \end{aligned} \right\} \quad (3.26)$$

Defined in terms of incremental velocity gradient as in Dal Corso *et al.* (2008), the incremental stress intensity factor for Mode I loading is

$$\dot{K}_{(\epsilon)I} = 2\mu \lim_{\hat{x}_1 \rightarrow l^+} \sqrt{2\pi(\hat{x}_1 - l)} \hat{v}_{2,2}(\hat{x}_1, \hat{x}_2 = 0) = 2\mu \hat{v}_{2,2}^\infty \sqrt{\pi l}, \quad (3.27)$$

resulting independent of the prestress parameters ξ , k and η (but μ may depend on the full set of current state variables) and of the angle ϑ_0 between the stiffener and the directions of principal stress T_1 .

The calculation of the incremental energy release rate and the incremental axial force in the stiffener (deferred to appendix A) generalizes results for a stiffener aligned parallel to the principal stress directions obtained by Bigoni *et al.* (2008) and Dal Corso *et al.* (2008). Those results can be now recovered by setting $\vartheta_0=0$ and thus obtaining

$$\left. \begin{aligned} D_1 = -D_2 &= -\frac{1}{2\alpha}, \quad \Gamma = 0, \quad \text{in EC} \\ D_1 = -D_2 &= -\frac{i}{\beta_1 - \beta_2}, \quad \Gamma = 0, \quad \text{in EI}, \end{aligned} \right\} \quad (3.28)$$

showing that in the case of a stiffener aligned parallel to prestress principal axes, there is no rigid rotation of the line due to the symmetry of the problem. The rigid rotation is null also in another case corresponding to $k=0$ (and $\{\vartheta_0, \eta\} \neq 0$)

$$D_1 = -D_2 = \frac{1}{2\sqrt{1-\xi}} (-\cos 2\vartheta_0 + i\sqrt{\xi} \sin 2\vartheta_0), \quad \Gamma = 0. \quad (3.29)$$

The normalized stiffener rotation Γ (3.24) is reported in figure 4, for a J_2 -deformation theory material, showing an antisymmetric behaviour with respect to the shear parameter γ . Note that results reported in figure 4 are independent of the hardening parameter N , except for the fact that the curve terminates at failure of ellipticity $\gamma^E = \gamma^E(N)$.

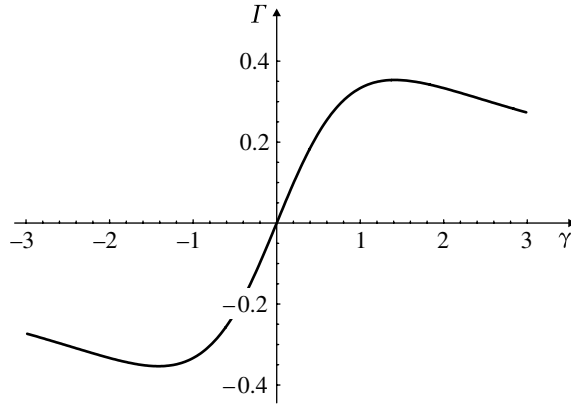


Figure 4. Normalized stiffener rotation $\Gamma = \omega_S / \dot{v}_{2,2}^\infty$ in a J_2 -deformation theory material generated by an incremental Mode I superimposed upon a simple shear of finite amount γ .

4. Incremental strain field near an inclined stiffener

The previously obtained solution can now be employed to analyse the incremental strain field near the stiffener. In particular, level sets of the modulus of perturbed incremental deviatoric strain for J_2 -deformation theory of plasticity are reported in figure 5 for (a,b) low $N=0.1$ and (c,d) high $N=0.8$ strain hardening.

For a J_2 -deformation theory material, the loss of ellipticity occurs at $\gamma^E=0.654$ for $N=0.1$ and at $\gamma^E=2.452$ for $N=0.8$. Two values of amount of shear γ have been considered in figure 5, namely, $\gamma=0$ corresponding to a material with null prestress⁷ and $\gamma \approx 0.95\gamma^E$, namely, close to the boundary of ellipticity loss, before the Mode I perturbation is applied.

When the perturbation is applied at high prestrain, the incremental deformation fields appear strongly focused along the near-tip directions of the shear bands formally possible at ellipticity loss, thus confirming the results of Bigoni *et al.* (2008). Moreover, the results pertaining to low strain hardening ($N=0.1$, figure 5b) show that the bands closest to the stiffener line are privileged, so that something resembling a ‘thick’ shear band parallel to the stiffener appears, a finding in qualitative agreement with the experimental results of Misra & Mandal (2007).

5. Incremental solution in the parabolic and hyperbolic regimes

Accepting non-decaying of the solution and an infinite strain (and stress) increment along certain shear band lines, the previously obtained solution can be extended to the parabolic and hyperbolic regimes. Since beyond the elliptic

⁷ At null prestress, the J_2 -deformation theory of plasticity becomes incrementally rigid (since both μ and μ_* tend to infinity, but their ratio ξ tends to N). It is expedient, therefore, to plot results normalized through division by μ , so that they tend to results pertaining to an incompressible orthotropic material deformed in small strain. The axes of orthotropy are therefore inclined at 45° with respect to the stiffener line in figure 5.

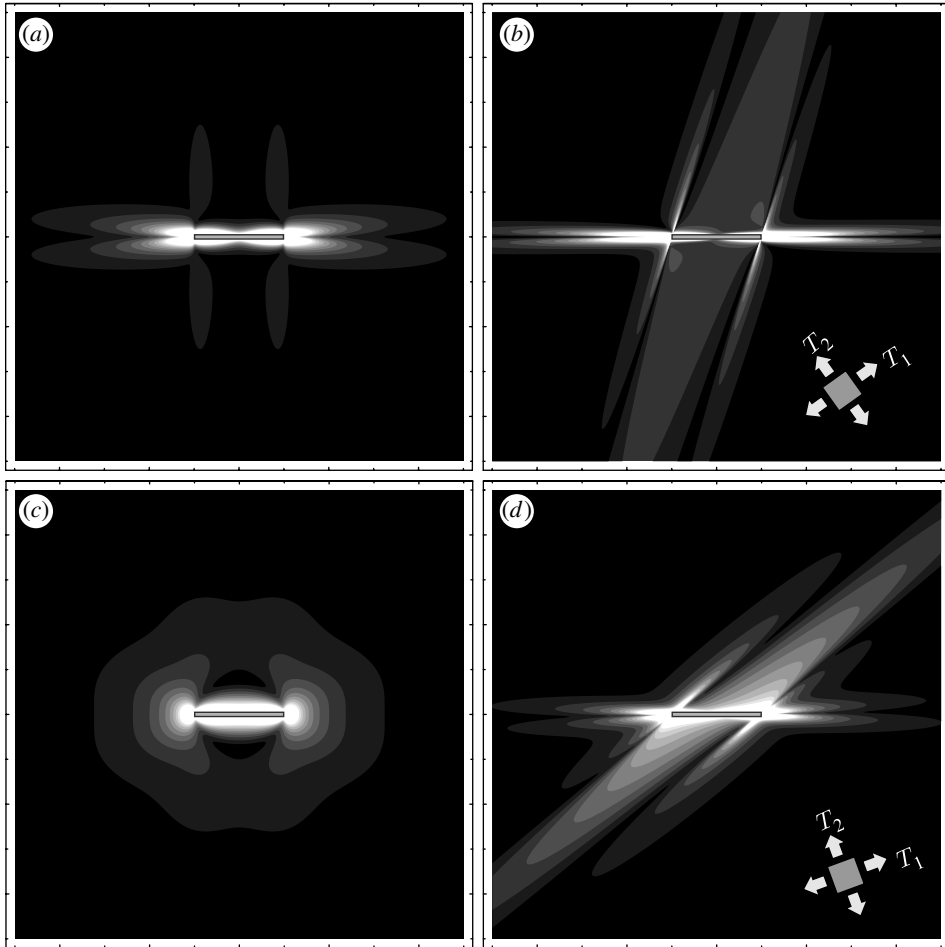


Figure 5. Level sets of the modulus of perturbed incremental deviatoric strain for a stiffener (evidenced with a thin rectangle, providing the bar scale of the representation) embedded in a J_2 -deformation theory material (with $(a,b) N=0.1$ and $(c,d) N=0.8$) subject to a finite simple shear of amount γ and a subsequent Mode I incremental uniform remote load. Null shear before the perturbation is considered in (a,c) , while a shear equal to 0.95 times the amount at ellipticity loss, γ^E , is considered in (b,d) . Note that the prestress (of principal components T_1 and T_2) generated through the shear deformation is inclined with respect to the stiffener line (and sketched in the figures).

range a problem is known to be ill-posed, the analysis of the solution within the parabolic and hyperbolic regimes is instructive to reveal features related to ill-posedness.

To obtain a solution (which need not be unique) beyond the elliptic range, we have to go back to the representation of the stream function (3.21), where the indices now have to range from 1 to n , so that

$$\hat{\psi}^\circ(\hat{x}_1, \hat{x}_2) = \frac{\hat{v}_{2,2}^\infty}{2} \sum_{j=1}^n \text{Re} \left\{ D_j \left[\hat{z}_j^2 - \hat{z}_j \sqrt{\hat{z}_j^2 - l^2} + l^2 \ln \left(\hat{z}_j + \sqrt{\hat{z}_j^2 - l^2} \right) \right] \right\}, \quad (5.1)$$

where n indicates the number of non-conjugate roots (i.e. $n=4$ ($n=3$) in $H(P)$).

Outside the elliptic regime, the characteristic lines defined as

$$\hat{z}_j = \text{const.} \Rightarrow \frac{d\hat{x}_2}{d\hat{x}_1} = -\frac{1}{W_j} \tag{5.2}$$

become real and correspond to four (two) different families in the hyperbolic (parabolic) regime and, in particular, their inclinations correspond to the following shear band inclinations:

$$\hat{\vartheta}_j = -\arctan\left[\frac{1}{W_j}\right] = \vartheta_0 - \arctan\left[\frac{1}{Q_j}\right], \tag{5.3}$$

where $j=1, \dots, 4$ in H ($j=1, 2$ in P).

The decaying of solution (5.1) is lost along the characteristic lines emanating from the stiffener tips, where, additionally, the increment of strain, and consequently stress, becomes infinite (while for the other characteristic lines cutting the stiffener the solution remains always bounded). By contrast, incremental displacements remain continuous and finite everywhere, even along characteristics.

The system of linear equations

$$\left. \begin{aligned} \sum_{j=1}^n \text{Re}[W_j]\text{Re}[D_j] - \text{Im}[W_j]\text{Im}[D_j] &= 1, \\ \sum_{j=1}^n \text{sign}[\text{Im}[Q_j]]\{\text{Im}[W_j]\text{Re}[D_j] + \text{Re}[W_j]\text{Im}[D_j]\} &= 0, \\ \sum_{j=1}^n \text{sign}[\text{Im}[Q_j]]\text{Im}[D_j] &= 0, \\ \sum_{j=1}^n \text{sign}[\text{Im}[Q_j]]\{-c_{2j}\text{Re}[D_j] + c_{1j}\text{Im}[D_j]\} &= 0, \end{aligned} \right\} \tag{5.4}$$

replaces system (3.22) to determine the n complex constants D_j , providing the solution. Note that the determination of these $2n$ real constants depend on four equations, so that ∞^{2n-4} solutions are possible.

Focusing attention to the hyperbolic regime, where $n=4$ and the roots W_j are real, the system (5.4) simplifies to

$$\left. \begin{aligned} \sum_{j=1}^4 W_j \text{Re}[D_j] &= 1, \\ \sum_{j=1}^4 W_j \text{Im}[D_j] &= 0, \\ \sum_{j=1}^4 \text{Im}[D_j] &= 0, \\ \sum_{j=1}^4 W_j^2 [2(\hat{\mathbb{K}}_{2221} - \hat{\mathbb{K}}_{2111}) - W_j \hat{\mathbb{K}}_{2121}] \text{Im}[D_j] &= 0, \end{aligned} \right\} \tag{5.5}$$

so that the general solution of linear system (5.5) can be written as

$$\begin{aligned} \begin{bmatrix} D_1 \\ D_2 \\ D_3 \\ D_4 \end{bmatrix} &= \zeta_1 \begin{bmatrix} 1 \\ 0 \\ 0 \\ 0 \end{bmatrix} + \zeta_2 \begin{bmatrix} 0 \\ 1 \\ 0 \\ 0 \end{bmatrix} + \zeta_3 \begin{bmatrix} 0 \\ 0 \\ 1 \\ 0 \end{bmatrix} + \frac{1 - \zeta_1 W_1 - \zeta_2 W_2 - \zeta_3 W_3}{W_4} \begin{bmatrix} 0 \\ 0 \\ 0 \\ 1 \end{bmatrix} \\ &+ i\chi \begin{bmatrix} (c_{14} - c_{13}) W_2 + (c_{12} - c_{14}) W_3 + (c_{13} - c_{12}) W_4 \\ (c_{13} - c_{14}) W_1 + (c_{14} - c_{11}) W_3 + (c_{11} - c_{13}) W_4 \\ (c_{14} - c_{12}) W_1 + (c_{11} - c_{14}) W_2 + (c_{12} - c_{11}) W_4 \\ (c_{12} - c_{13}) W_1 + (c_{13} - c_{11}) W_2 + (c_{11} - c_{12}) W_3 \end{bmatrix}, \end{aligned} \tag{5.6}$$

where $\zeta_1, \zeta_2, \zeta_3$ and χ are arbitrary real constants.

Since system (5.5) admits ∞^4 solutions, we have chosen to represent in figure 6 the deformed shape of an area near the stiffener, for the four solutions corresponding (from left to right and from the upper to the lower part) to index h ranging between 1 and 4 so that⁸

$$D_h = \frac{1}{W_h}, \quad D_j = 0, \quad j \neq h, \quad j \in [1, 4]. \tag{5.7}$$

We can note from figure 6 that for given uniform Mode I remote loading of a stiffener embedded in a medium uniformly prestrained beyond the elliptic range:

- (i) an infinite number of solutions is possible,
- (ii) these solutions do not decay at infinity,
- (iii) they correspond to infinite incremental strain and stress along shear bands, and
- (iv) these shear bands emanate from the tips of the stiffener.

The above conclusion, based on an analytical solution, explains the difficulties typically encountered in the numerical analyses of ill-posed boundary-value problems.

6. Conclusions

An incremental solution has been given for uniform Mode I perturbation of a rigid, thin inclusion in an infinite (incompressible) elastic material, subject to uniform prestress with principal axes inclined with respect to the inclusion line.

⁸The values in (5.7) are achievable for $\chi=0$,

$$\zeta_h = \frac{1}{W_h}, \quad \zeta_k = 0, \quad k \neq h, \quad \text{if } h = 1, 2, 3$$

and

$$\zeta_1 = \zeta_2 = \zeta_3 = 0, \quad \text{if } h = 4.$$

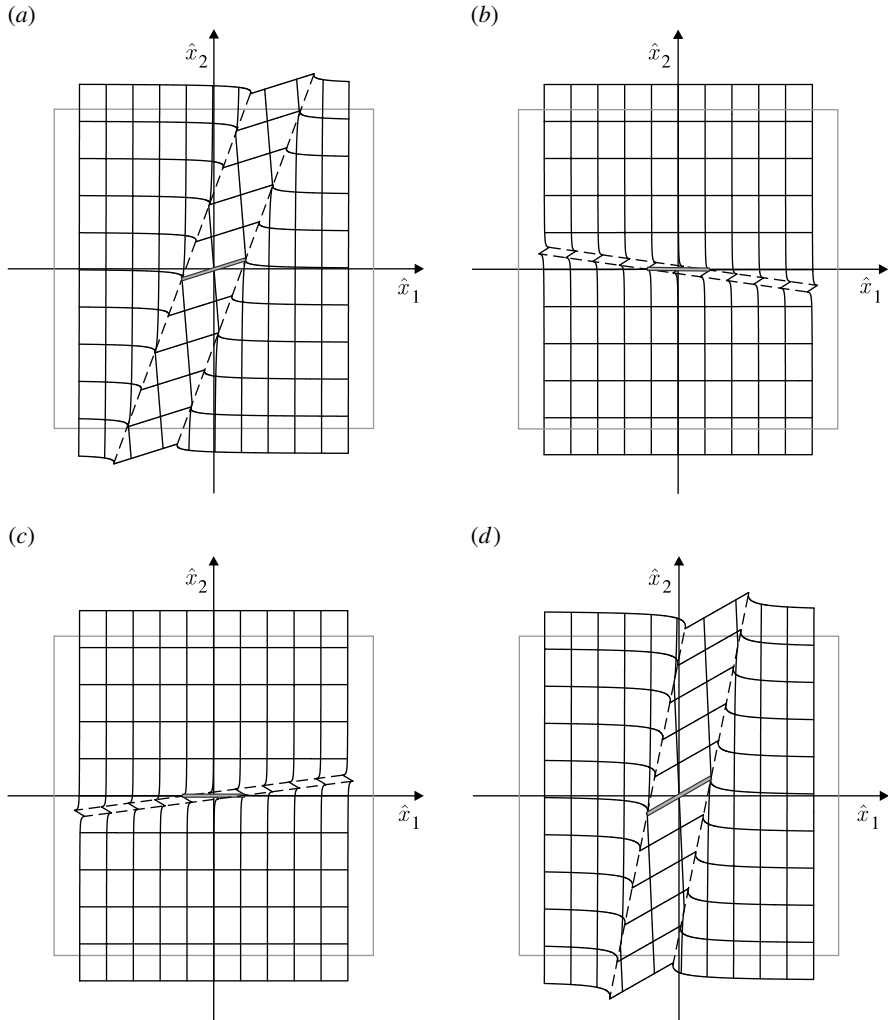


Figure 6. Deformed configurations (the grey square represents the undeformed, prestressed material) for a stiffener (evidenced with a thin rectangle, providing the bar scale of the representation) embedded in a J_2 -deformation theory material (with $N=0.1$, subject to a finite shear of amount $\gamma=1.2\gamma^E$) and a subsequent Mode I incremental uniform remote load. Four solutions are reported among the ∞^4 possible *within the hyperbolic range*, where characteristics are inclined at $\{(a) 62.984^\circ, (b) -5.874^\circ, (c) 5.434^\circ, (d) 74.292^\circ\}$, with respect to the \hat{x}_1 -axis.

The obtained results conclude an investigation initially limited to coaxiality between the prestress principal axes and the inclusion line (Bigoni *et al.* 2008; Dal Corso *et al.* 2008). It is shown, in particular, that the initial state of uniform prestress can be obtained through a finite simple shear parallel to the inclusion line and that the amount of shear may be sufficient to bring the state of stress as close as possible the elliptic boundary and even beyond it, namely, within the hyperbolic or parabolic regimes. The obtained results therefore allow analytical investigations of the interactions between a rigid inclusion and shear bands and reveal a tendency towards a focusing of the shear bands parallelly to the

stiffener line. Finally, extending the solution beyond the elliptic regime, it has been shown that the fields do not decay, carry an infinite strain rate within the shear bands and that there exist ∞^4 (∞^2) solutions in the hyperbolic (parabolic) regime. These results analytically highlight the well-known numerical difficulties encountered in the analysis of boundary-value problems beyond the elliptic range.

Financial support of MIUR-Prin 2007 (prot. 2007YZ3B24_002) is gratefully acknowledged.

Appendix A. Incremental energy release rate for stiffener growth and axial force along the stiffener

Analogously to Bigoni *et al.* (2008, §3), we analyse the possibility of incremental stiffener growth and its related incremental energy release rate. Briefly, the incremental energy release rate for a rectilinear growth can be expressed as

$$\dot{G}_I = - \lim_{\Delta l \rightarrow 0} \frac{1}{2\Delta l} \int_0^{\Delta l} \llbracket \hat{t}_{2i}(\Delta l - r, \pi) \rrbracket \hat{v}_i(r, 0) dr, \tag{A 1}$$

where (the repeated index is summed and) the asymptotic fields are expressed in the polar coordinate system (r, ϑ) centred at the stiffener tip ($\hat{x}_1 = l, \hat{x}_2 = 0$), so that r denotes the radial distance from the stiffener tip and ϑ indicates values of the polar coordinate (anticlockwise) angle singling out r from the \hat{x}_1 -axis (so that $\vartheta = 0$ corresponds to points ahead of the stiffener tip). The asymptotic fields result in (constant terms have been neglected)

$$\left. \begin{aligned} \llbracket \hat{t}_{21}(\Delta l - r, \pi) \rrbracket &= -\hat{v}_{2,2}^\infty \frac{\sqrt{2l}}{\sqrt{\Delta l - r}} \hat{\mathbb{K}}_{2121} \text{Im}[W_1^2 D_1 + W_2^2 D_2], \\ \llbracket \hat{t}_{22}(\Delta l - r, \pi) \rrbracket &= -\hat{v}_{2,2}^\infty \frac{\sqrt{2l}}{\sqrt{\Delta l - r}} \{2(\hat{\mathbb{K}}_{2221} - \hat{\mathbb{K}}_{2111}) \text{Im}[W_1^2 D_1 + W_2^2 D_2] \\ &\quad - \hat{\mathbb{K}}_{2121} \text{Im}[W_1^3 D_1 + W_2^3 D_2]\}, \\ \hat{v}_1(r, 0) &= -\hat{v}_{2,2}^\infty \sqrt{2lr} \\ \hat{v}_2(r, 0) &= -\Gamma \hat{v}_{2,2}^\infty \sqrt{2lr}, \end{aligned} \right\} \tag{A 2}$$

and

from which the incremental energy release rate for stiffener growth can be calculated in the form

$$\begin{aligned} \dot{G}_I &= - \frac{\dot{K}^{(\epsilon)I 2}}{8\mu^2} \{ [\hat{\mathbb{K}}_{2121} + 2\Gamma(\hat{\mathbb{K}}_{2221} - \hat{\mathbb{K}}_{2111})] \text{Im}[W_1^2 D_1 + W_2^2 D_2] \\ &\quad - \Gamma \hat{\mathbb{K}}_{2121} \text{Im}[W_1^3 D_1 + W_2^3 D_2] \}. \end{aligned} \tag{A 3}$$

We have numerically checked that \dot{G}_I is (i) independent of η and (ii) always negative in the elliptic regime, so that stiffener reduction is predicted.

The behaviour of the incremental energy release rate for a stiffener embedded in a J_2 -deformation theory material is reported in figure 7 as a function of the

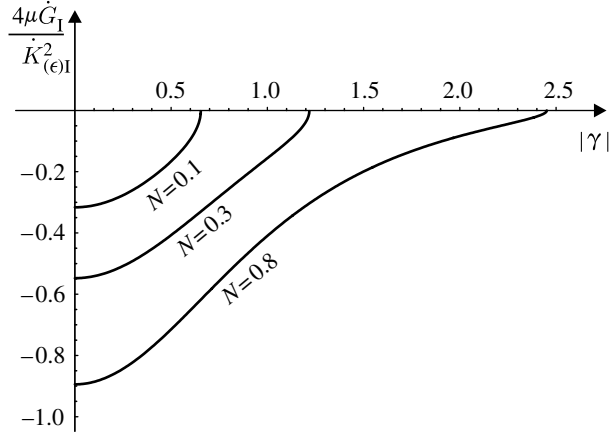


Figure 7. Mode I incremental energy release rate for a stiffener embedded in a J_2 -deformation theory material subjected to a finite shear parallel to the stiffener line and defined by the shear amount parameter γ . Different hardening parameters N are considered.

amount of shear γ , for different values of the hardening parameter N . It should be noted from the figure that the maximum of the curves always occurs at null shear $\gamma=0$ for every N , and that at ellipticity loss the incremental energy release rate vanishes, so that stiffener reduction is inhibited.

Note that μ is a function of γ and, in particular, μ tends to infinity when γ tends to zero. We have selected to normalize the plot through multiplication by $\mu/\hat{K}_{(\epsilon)I}^2$ to recover linear elasticity results in the special case of the absence of prestress (where the J_2 -deformation theory of plasticity loses meaning and our plot refers to an elastic orthotropic material with orthotropy axes inclined at 45° with respect to the stiffener line).

The incremental axial force in the stiffener can be calculated from equation (3.18)₁ where the jump of the perturbed shear nominal traction increment can be evaluated to be

$$\llbracket \hat{t}_{21}(\hat{x}_1, 0) \rrbracket = -2\hat{v}_{2,2}^\infty \hat{K}_{2121} \text{Im} [W_1^2 D_1 + W_2^2 D_2] \frac{\hat{x}_1}{\sqrt{l^2 - \hat{x}_1^2}}, \quad \forall |\hat{x}_1| < l, \quad (\text{A } 4)$$

so that, using the identity (3.25) (which has only been numerically checked to hold), the incremental axial force in the stiffener related to a Mode I loading is

$$\hat{\mathcal{N}}(\hat{x}_1) = -2\hat{v}_{2,2}^\infty \hat{K}_{2121} \text{Im} [W_1 + W_2 + \Gamma W_1 W_2] \sqrt{l^2 - \hat{x}_1^2}, \quad \forall |\hat{x}_1| < l, \quad (\text{A } 5)$$

resulting again independent of the in-plane mean stress, parameter η .

Note that the maximum of the axial force always occurs at the stiffener centre and we have numerically verified that the incremental maximum axial force is related to the incremental energy release rate as

$$\dot{G}_I = \frac{\pi \hat{v}_{2,2}^\infty}{4} \dot{\mathcal{N}}_{\max}, \quad (\text{A } 6)$$

which is always negative in the elliptic regime, so that the stiffener is subject to compression for positive $\hat{v}_{2,2}^\infty$.

Appendix B. Solution for a prescribed rigid rotation of a stiffener in a prestressed medium

We consider the problem of a stiffener subject to a prescribed incremental rotation ω_S and embedded in a homogeneously prestressed material. This problem may, for instance, find application to the interpretation of the so-called ‘vane test’ used in geotechnical engineering. Imposing the satisfaction of the kinematical boundary conditions along the stiffener line (3.19), where now ω_S is prescribed, we represent the stream function as

$$\hat{\psi}^\circ(\hat{x}_1, \hat{x}_2) = \frac{\omega_S}{2} \sum_{j=1}^2 \operatorname{Re} \left\{ E_j^{\text{II}} \left[\hat{z}_j^2 - \hat{z}_j \sqrt{\hat{z}_j^2 - l^2} + l^2 \ln \left(\hat{z}_j + \sqrt{\hat{z}_j^2 - l^2} \right) \right] \right\}, \quad (\text{B } 1)$$

which yields the following linear problem for the complex constants E_1^{II} and E_2^{II} :

$$\begin{bmatrix} \operatorname{Re}[W_1] & -\operatorname{Im}[W_1] & \operatorname{Re}[W_2] & -\operatorname{Im}[W_2] \\ \operatorname{Im}[W_1] & \operatorname{Re}[W_1] & \operatorname{Im}[W_2] & \operatorname{Re}[W_2] \\ 1 & 0 & 1 & 0 \\ 0 & 1 & 0 & 1 \end{bmatrix} \begin{bmatrix} \operatorname{Re}[E_1^{\text{II}}] \\ \operatorname{Im}[E_1^{\text{II}}] \\ \operatorname{Re}[E_2^{\text{II}}] \\ \operatorname{Im}[E_2^{\text{II}}] \end{bmatrix} = \begin{bmatrix} 0 \\ 0 \\ -1 \\ 0 \end{bmatrix}. \quad (\text{B } 2)$$

The solution of the present problem does not depend on the in-plane stress parameter η , similar to the solution (3.22), and satisfies

$$W_1^2 E_1^{\text{II}} + W_2^2 E_2^{\text{II}} = W_1 W_2 \quad \text{and} \quad W_1^3 E_1^{\text{II}} + W_2^3 E_2^{\text{II}} = W_1 W_2 (W_1 + W_2). \quad (\text{B } 3)$$

In the particular case of $\vartheta_0=0$, the solution becomes

$$\left. \begin{aligned} E_1^{\text{II}} &= -\frac{1}{2\alpha}(\alpha + i\beta), \quad E_2^{\text{II}} = -\frac{1}{2\alpha}(\alpha - i\beta) \Rightarrow \operatorname{Im}[W_1^2 E_1^{\text{II}} + W_2^2 E_2^{\text{II}}] = 0, \quad \text{in EC} \\ \text{and} \\ E_1^{\text{II}} &= \frac{\beta_2}{\beta_1 - \beta_2}, \quad E_2^{\text{II}} = -\frac{\beta_1}{\beta_1 - \beta_2} \Rightarrow \operatorname{Im}[W_1^2 E_1^{\text{II}} + W_2^2 E_2^{\text{II}}] = 0, \quad \text{in EI.} \end{aligned} \right\} \quad (\text{B } 4)$$

We now define the incremental stress intensity factor as

$$\dot{K}_{(\epsilon)\text{II}} = 2\mu \lim_{\hat{x}_1 \rightarrow l^+} \sqrt{2\pi(\hat{x}_1 - l)} \hat{v}_{2,1}(\hat{x}_1, \hat{x}_2 = 0) = -2\mu\omega_S \sqrt{\pi l} \quad (\text{B } 5)$$

and the incremental energy release rate as

$$\dot{G}_{\text{II}} = -\lim_{\Delta l \rightarrow 0} \frac{1}{2\Delta l} \int_0^{\Delta l} \llbracket \hat{t}_{2i}(\Delta l - r, \pi) \rrbracket \hat{v}_i(r, 0) dr, \quad (\text{B } 6)$$

where the asymptotic fields in the polar coordinate system (r, ϑ) centred at the stiffener tip ($\hat{x}_1 = l, \hat{x}_2 = 0$) are (constant terms have been neglected)

$$\left. \begin{aligned} \llbracket \hat{t}_{21}(\Delta l - r, \pi) \rrbracket &= -\omega_S \frac{\sqrt{2l}}{\sqrt{\Delta l - r}} \hat{\mathbb{K}}_{2121} \operatorname{Im}[W_1^2 E_1^{\text{II}} + W_2^2 E_2^{\text{II}}], \\ \llbracket \hat{t}_{22}(\Delta l - r, \pi) \rrbracket &= -\omega_S \frac{\sqrt{2l}}{\sqrt{\Delta l - r}} \{ 2(\hat{\mathbb{K}}_{2221} - \hat{\mathbb{K}}_{2111}) \operatorname{Im}[W_1^2 E_1^{\text{II}} + W_2^2 E_2^{\text{II}}] \\ &\quad - \hat{\mathbb{K}}_{2121} \operatorname{Im}[W_1^3 E_1^{\text{II}} + W_2^3 E_2^{\text{II}}] \}, \\ \hat{v}_1(r, 0) &= 0 \quad \text{and} \quad \hat{v}_2(r, 0) = -\omega_S \sqrt{2lr}. \end{aligned} \right\} \quad (\text{B } 7)$$

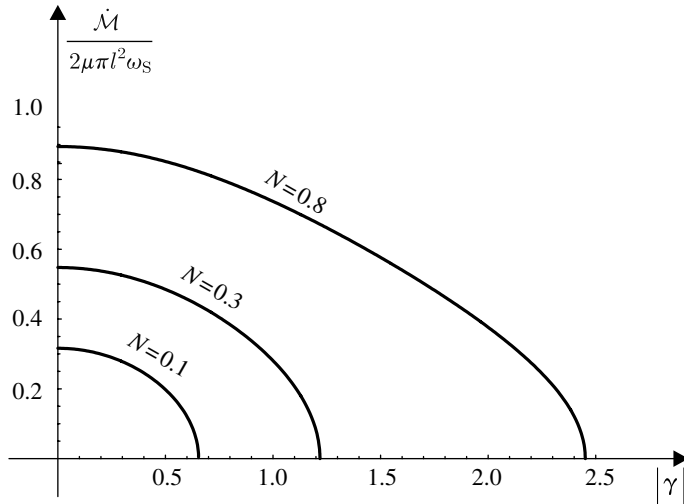


Figure 8. Incremental moment $\dot{\mathcal{M}}$ for an incremental rotation ω_S of the stiffener as a function of the simple shear amplitude γ , for a J_2 -deformation theory material at different values of strain hardening coefficient N .

Using the identity (B 3), the incremental energy release rate for stiffener growth (B 6) can be calculated in the form

$$\dot{G}_{II} = -\frac{\dot{K}^{(\epsilon)II 2}}{8\mu^2} \{2(\hat{\mathbb{K}}_{2221} - \hat{\mathbb{K}}_{2111})\text{Im}[W_1 W_2] - \hat{\mathbb{K}}_{2121}\text{Im}[W_1 W_2(W_1 + W_2)]\}, \quad (\text{B } 8)$$

which has been numerically checked to be always negative in the elliptic regime. The incremental global axial and shear forces can be computed and are null by equilibrium, while the incremental moment applied to the inclusion (taken positive when anticlockwise) is given by

$$\begin{aligned} \dot{\mathcal{M}} &= -\int_{-l}^l \llbracket \hat{t}_{22}(y, 0) \rrbracket y \, dy \\ &= \pi l^2 \omega_S \{2(\hat{\mathbb{K}}_{2221} - \hat{\mathbb{K}}_{2111})\text{Im}[W_1 W_2] - \hat{\mathbb{K}}_{2121} \text{Im}[W_1 W_2(W_1 + W_2)]\}, \quad (\text{B } 9) \end{aligned}$$

which corresponds, when prestress is absent, to the value $2\mu\pi l^2\omega_S$ calculated by Muskhelishvili (1953, §83a). Note that the following interesting relation holds true in the elliptic regime:

$$\dot{G}_{II} = -\frac{\dot{\mathcal{M}}\omega_S}{2l}, \quad (\text{B } 10)$$

from which, due to the negativity of \dot{G}_{II} , we note that $\dot{\mathcal{M}}$ has always the same sign of ω_S .

The incremental moment and level sets of incremental deviatoric strain are reported as functions of the simple shear amplitude γ in figures 8 and 9, for a J_2 -deformation theory material at different values of strain hardening coefficient N . In particular, we note that the maximum incremental moment divided by μ occurs at null prestress, while at the ellipticity loss, the incremental moment vanishes and the shear bands near the direction orthogonal to the stiffener are privileged.

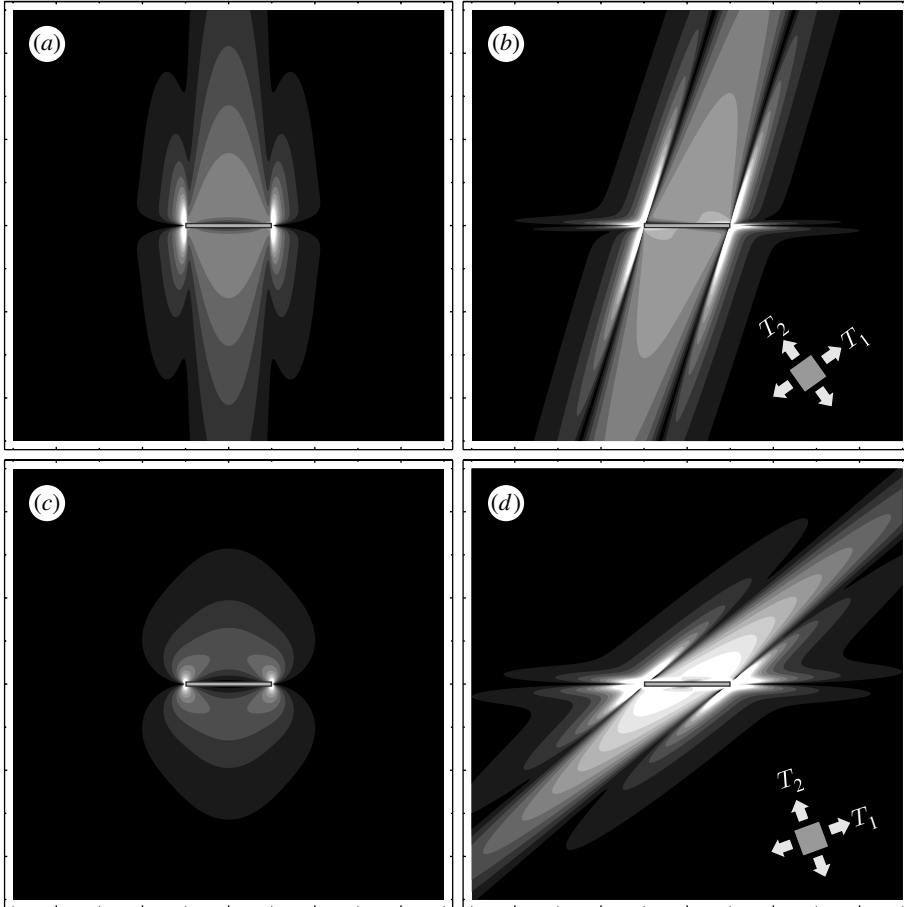


Figure 9. Level sets of the modulus of perturbed incremental deviatoric strain for a stiffener (evidenced with a thin rectangle, providing the bar scale of the representation) embedded in a J_2 -deformation theory material (with (a,b) $N=0.1$ and (c,d) $N=0.8$) subject to a finite shear of amount γ and a subsequent imposed incremental rigid rotation ω_S . Null shear before the perturbation is considered in (a,c), while a shear equal to 0.95 times the amount at ellipticity loss, γ^E , is considered in (b,d). Note that the prestress (of principal components T_1 and T_2) generated through the simple shear deformation is inclined with respect to the stiffener line.

References

- Bigoni, D. & Dal Corso, F. 2008 The unrestrainable growth of a shear band in a prestressed material. *Proc. R. Soc. A* **464**, 2365–2390. (doi:10.1098/rspa.2008.0029)
- Bigoni, D., Dal Corso, F. & Gei, M. 2008 The stress concentration near a rigid line inclusion in a prestressed, elastic material. Part II. Implications on shear band nucleation, growth and energy release rate. *J. Mech. Phys. Solids* **56**, 839–857. (doi:10.1016/j.jmps.2007.07.003)
- Dal Corso, F., Bigoni, D. & Gei, M. 2008 The stress concentration near a rigid line inclusion in a prestressed, elastic material. Part I. Full-field solution and asymptotics. *J. Mech. Phys. Solids* **56**, 815–838. (doi:10.1016/j.jmps.2007.07.002)

- Harren, S., Lowe, T. C., Asaro, R. J. & Needleman, A. 1989 Analysis of large-strain shear in rate-dependent face-centred cubic polycrystals: correlation of micro- and macromechanics. *Phil. Trans. R. Soc. A* **328**, 443–500. (doi:10.1098/rsta.1989.0048)
- Misra, S. & Mandal, N. 2007 Localization of plastic zones in rocks around rigid inclusions: insights from experimental and theoretical models. *J. Geophys. Res.* **112**, B09 206. (doi:10.1029/2006JB004328)
- Muskhelishvili, N. I. 1953 *Some basic problems of the mathematical theory of elasticity*. Groningen, The Netherlands: P. Noordhoff Ltd.
- Öztürk, T., Poole, W. J. & Embury, J. D. 1991 The deformation of Cu–W laminates. *Mater. Sci. Eng. A* **148**, 175–178. (doi:10.1016/0921-5093(91)90819-9)
- Weissenberg, K. 1948 Abnormal substances and abnormal phenomena of flow. In *Proc. Int. Congr. Rheology*, pp. I-29–I-46.